The Journal of Chemical Physics

# Flow-induced scission of wormlike micelles in nonionic surfactant solutions under shear flow

Cite as: J. Chem. Phys. **157**, 084903 (2022); https://doi.org/10.1063/5.0096830
Submitted: 22 April 2022 • Accepted: 21 July 2022 • Accepted Manuscript Online: 25 July 2022 • Published Online: 30 August 2022

Yusuke Koide and Susumu Goto







AIP Publishing

The Journal of Chemical Physics ARTICLE scitation.org/journal/jcp

# Flow-induced scission of wormlike micelles in nonionic surfactant solutions under shear flow

Cite as: J. Chem. Phys. 157, 084903 (2022); doi: 10.1063/5.0096830
Submitted: 22 April 2022 • Accepted: 21 July 2022 •
Published Online: 30 August 2022



Yusuke Koide[a] and Susumu Goto[b]

## AFFILIATIONS

Graduate School of Engineering Science, Osaka University, 1-3 Machikaneyama, Toyonaka, Osaka 560-8531, Japan

[a]Author to whom correspondence should be addressed: y_koide@fm.me.es.osaka-u.ac.jp
[b]Electronic mail: s.goto.es@osaka-u.ac.jp

## ABSTRACT

We investigate flow-induced scission of wormlike micelles with dissipative particle dynamics simulations of nonionic surfactant solutions under shear flow. To understand flow-induced scission in terms of micellar timescales, we propose a method to evaluate the longest relaxation time of unentangled surfactant micelles from the rotational relaxation time and the average lifetime at equilibrium. The mean squared displacement of surfactant molecules provides evidence that the longest relaxation time estimated by the proposed method serves as the characteristic timescale at equilibrium. We also demonstrate that the longest relaxation time plays an essential role in flow-induced scission. Using conditional statistics based on the aggregation number of micelles, we examine the statistical properties of the lifetime of wormlike micelles. We then conclude that flow-induced scission occurs when the Weissenberg number defined as the product of the longest relaxation time and the shear rate is larger than a threshold value.



## I. INTRODUCTION

Surfactants consist of hydrophilic and hydrophobic moieties. Above a critical concentration, surfactants spontaneously assemble into aggregates such as spherical micelles, rodlike micelles, and wormlike micelles in aqueous solutions.[1] Since these micelles exhibit unique properties, they can serve as additives in working fluids for various applications, including rheology control,[2] turbulent drag reduction,[3] and drug delivery systems.[4] Therefore, it is crucial to understand the structures and dynamics of micelles in flowing solutions for industrial applications of surfactants.

Flow-induced scission of surfactant micelles is among the crucial phenomena. Although thermal fluctuations induce scission of micelles at equilibrium, flow with high velocity gradients promotes their scission.[5–7] This phenomenon may be intuitively obvious, but it is difficult to quantitatively predict the conditions and degree of flow-induced scission, which are required for practical use of surfactants. An increase in scission frequency brings about a drastic change in micellar structures and distributions, leading to a significant modification of the flow properties of surfactant solutions.[6,8–10] In addition, since the constitutive equations for surfactant solutions need to include the effect of scission and recombination kinetics explicitly,[11–13] insight into flow-induced micellar scission leads to an understanding of the rheology and turbulent drag reduction phenomenon of surfactant solutions. In other words, to reveal the macroscopic flow behavior of surfactant solutions, we need to understand the properties of flow-induced micellar scission. In the present study, we focus on a uniform shear flow, which is often used in rheological measurements, and investigate flow-induced scission of wormlike surfactant micelles in detail.

Although some experimental studies succeeded in evaluating the average lifetime of micelles,[14–16] it is difficult to experimentally observe the structures and dynamics of individual micelles in flowing solutions. Molecular simulations allow us to overcome this difficulty with measurements. When we are interested in the slow dynamics of micelles rather than the fast dynamics at the atomic level, coarse-graining, in which several atoms or molecules are considered as a single particle, is often used to reduce the computational cost associated with all-atom molecular dynamics simulations. The coarse-grained molecular dynamics (CGMD) method using the MARTINI force field is one of the most popular approaches based on coarse-graining. With CGMD, we can simulate micellar scission to evaluate relevant micellar properties directly.[17,18] Regarding flow-induced scission, Sambasivam *et al.*[19] conducted CGMD simulations of a single rodlike micelle under shear flow and found that elongation of micelles by a shear flow increased the potential energy,

thus leading to the scission of micelles. Although CGMD simulations have revealed the detailed dynamics of micellar scission, many studies simulated a single micelle or a few micelles only.[17–19] Therefore, the statistical properties of flow-induced scission and its effect on the micellar distribution remain unclear.

Another coarse-graining approach relies on the introduction of a kinetic model for scission and recombination, and several models[20–22] have been proposed. These models significantly reduce the computational cost and allow systematic investigation of the statistical properties of scission and recombination. Kröger and Makhloufi[20] proposed the FENE-C model, which introduces scission and recombination into a finitely extensible nonlinear elastic (FENE) potential. They reported the shear-rate dependence of the average micellar length and lifetime under shear flow. Padding *et al.*[22] modeled a wormlike micelle as a string of thin rods and found that the average breaking rate varied depending on the scission energy and shear rate $\dot{\gamma}$. However, there is still room for consideration of these results concerning flow-induced scission because scission and recombination were explicitly modeled in these previous studies. Moreover, the explanation of the shear-rate dependence of flow-induced scission was unsatisfactory because relevant timescales of individual micelles were not considered.

It is well known that the relaxation time of micelles, which repeatedly break and recombine, is sometimes affected by scission. Regarding entangled micelles, Cates[23] proposed a theory that predicts the relaxation time from the average lifetime and reptation time of micelles. On the other hand, for unentangled micelles, Faivre and Gardissat[24] proposed a theory that incorporated the process of scission and recombination into the Rouse model, although they aimed at describing the viscoelasticity of amorphous selenium. Huang *et al.*[25] numerically confirmed the validity of this theory. According to the concept proposed by Faivre and Gardissat, Huang *et al.* defined the relaxation time $\tau_\Lambda$ of micelles, which corresponds to the relaxation time of a segment of size $\Lambda$ for which the lifetime is equal to the Rouse relaxation time. They found that chain deformation, orientation, and rheological properties under shear flow are expressed by universal functions of the dimensionless number $\beta_\Lambda = \tau_\Lambda \dot{\gamma}$. However, their simulations used a mesoscopic model incorporating a kinetic model for scission and recombination into linear chains. To our knowledge, no study has examined whether $\tau_\Lambda$ also plays a crucial role in unentangled micelles composed of surfactant molecules. Since surfactant micelles have complicated internal structures compared with polymer-like linear chains, they exhibit complex dynamics of scission and recombination. Therefore, the applicability of $\tau_\Lambda$ to surfactant micelles is not obvious and is worth studying.

In the present study, we intend to quantitatively reveal the shear-rate dependence of micellar scission and identify the timescales relevant to flow-induced scission. For this purpose, we conduct molecular simulations of nonionic surfactant solutions using the dissipative particle dynamics (DPD) method. DPD was proposed by Hoogerbrugge and Koelman[26] and then improved by Español and Warren.[27] Many researchers[28–34] have extensively investigated surfactant solutions using the DPD method. Since particles interact via soft repulsive interactions in DPD, we can make time steps larger than CGMD, which allows us to simulate large systems for long timescales with a low computational cost. Therefore, we can evaluate the statistical properties of flow-induced scission and its effect on the micellar distribution. Since previous studies[20,22,25] have analyzed the average properties over all the micelles in the system, their results could demonstrate only the combined effect of the changes in micellar properties and distributions. We overcome this problem using conditional statistics based on the aggregation number of micelles, which offer deeper insight into the shear flow effect on individual micelles. In addition, we introduce the longest relaxation time of unentangled micelles to demonstrate that a single dimensionless number can characterize flow-induced scission. More concretely, we extend the theory of Faivre and Gardissat[24] to unentangled surfactant micelles. We then prove the importance of this timescale in micellar scission under shear flow using the simulation results for various temperatures.

## II. SIMULATION METHOD

### A. DPD governing equations

In DPD simulations, we regard a group of atoms and molecules as a single DPD particle. The motion of a DPD particle obeys

$$m_i \frac{\mathrm{d}\boldsymbol{v}_i}{\mathrm{d}t} = \sum_{j(\neq i)} \boldsymbol{F}_{ij}^C + \sum_{j(\neq i)} \boldsymbol{F}_{ij}^D + \sum_{j(\neq i)} \boldsymbol{F}_{ij}^R, \tag{1}$$

where $m_i$ and $\boldsymbol{v}_i$ are the mass and velocity of the $i$th particle, respectively, and $\boldsymbol{F}_{ij}^C, \boldsymbol{F}_{ij}^D$, and $\boldsymbol{F}_{ij}^R$ are the conservative, dissipative, and random forces exerted on the $i$th particle by the $j$th particle, respectively. The conservative force acts as a repulsive force in the form of

$$\boldsymbol{F}_{ij}^C = \begin{cases} a_{ij}\left(1 - \dfrac{r_{ij}}{r_c}\right)\boldsymbol{e}_{ij} & \text{for } r_{ij} \le r_c, \\ 0 & \text{for } r_{ij} > r_c, \end{cases} \tag{2}$$

where $a_{ij}$ is the conservative force coefficient between the $i$th and $j$th particles, $r_c$ is the cutoff distance, $\boldsymbol{r}_{ij} = \boldsymbol{r}_i - \boldsymbol{r}_j, r_{ij} = |\boldsymbol{r}_{ij}|$, and $\boldsymbol{e}_{ij} = \boldsymbol{r}_{ij}/r_{ij}$ with $\boldsymbol{r}_i$ being the position of the $i$th particle. The dissipative and random forces are expressed as

$$\boldsymbol{F}_{ij}^D = -\gamma w^D(r_{ij})(\boldsymbol{e}_{ij} \cdot \boldsymbol{v}_{ij})\boldsymbol{e}_{ij} \quad (\boldsymbol{v}_{ij} = \boldsymbol{v}_i - \boldsymbol{v}_j) \tag{3}$$

and

$$\boldsymbol{F}_{ij}^R = \sigma w^R(r_{ij})\theta_{ij}\boldsymbol{e}_{ij}, \tag{4}$$

where $\gamma$ and $\sigma$ are the dissipative and random force coefficients, respectively, and $w^D(r_{ij})$ and $w^R(r_{ij})$ are the weight functions of the dissipative and random forces, respectively. In Eq. (4), $\theta_{ij}$ is a random variable that satisfies

$$\theta_{ij}(t) = \theta_{ji}(t), \tag{5}$$

$$\langle \theta_{ij}(t) \rangle = 0, \tag{6}$$

$$\langle \theta_{ij}(t)\theta_{kl}(t') \rangle = (\delta_{ik}\delta_{jl} + \delta_{il}\delta_{jk})\delta(t - t'), \tag{7}$$

where $\delta_{ij}$ is the Kronecker delta, $\delta(t)$ is the delta function, and $\langle \cdot \rangle$ denotes the ensemble average. The fluctuation dissipation theorem requires that $\gamma$, $\sigma$, $w^D(r_{ij})$, and $w^R(r_{ij})$ satisfy

$$w^D(r_{ij}) = \left[w^R(r_{ij})\right]^2 \tag{8}$$

and

$$\sigma^2 = 2\gamma k_B T, \tag{9}$$

where $k_B$ is the Boltzmann constant and $T$ is the temperature of the system.[27] Following Ref. 35, we set the weight function $w^R(r_{ij})$ as

$$w^R(r_{ij}) = \begin{cases} 1 - \dfrac{r_{ij}}{r_c} & \text{for } r_{ij} \le r_c, \\ 0 & \text{for } r_{ij} > r_c. \end{cases} \tag{10}$$

In what follows, we use simulation units with $k_B T_0 = m = r_c = 1$, where $T_0$ is the reference temperature.

## B. Surfactant model

The system is composed of water and nonionic surfactants. Since we focus on the general properties of flow-induced scission, we do not assume any specific species of surfactant molecule in the following. As shown in Fig. 1, a surfactant molecule contains a hydrophilic particle and two hydrophobic particles, which are connected by harmonic springs expressed by

$$\boldsymbol{F}_{ij}^B = -k_s(r_{ij} - r_{\mathrm{eq}})\boldsymbol{e}_{ij}, \tag{11}$$

where $k_s$ is the spring constant and $r_{\mathrm{eq}}$ is the equilibrium bond distance. We show the simulation parameters in Table I. Here, $N$ is the total number of DPD particles, $\rho$ is the number density of DPD particles, $\phi$ is the volume fraction of surfactants, and $a_{\mathrm{ij}}$ is the conservative force coefficient between different types of particles. The subscripts indicate the types of particles: h, t, and w denote the head, tail, and water particles, respectively. Here, we determine $a_{\mathrm{ij}}$ according to Ref. 36 because wormlike micelles are found to be formed for this model above a certain volume fraction. We choose $\phi = 0.05$ for a sufficient number of wormlike micelles to exist in the system. For a specific species of surfactant molecule, $a_{\mathrm{ij}}$ can be obtained using a parameterization scheme.[35,37–39] When we vary $k_B T$, $\gamma$ changes so that it satisfies Eq. (9) while fixing the value of $\sigma$ at 3.

**TABLE I.** DPD simulation parameters. $N$ is the total number of DPD particles, $\rho$ is the number density of DPD particles, $\sigma$ is the random force coefficient, $\phi$ is the volume fraction of surfactants, $k_s$ is the spring constant, $r_{\mathrm{eq}}$ is the equilibrium bond distance, and $a_{\mathrm{ij}}$ is the conservative force coefficient between different types of particles. The subscripts indicate the types of particles: h, t, and w denote head, tail, and water particles, respectively.

| $N$ | $\rho$ | $\sigma$ | $\phi$ | $k_s$ | $r_{\mathrm{eq}}$ | $a_{\mathrm{hh}}$ | $a_{\mathrm{ht}}$ | $a_{\mathrm{hw}}$ | $a_{\mathrm{tt}}$ | $a_{\mathrm{tw}}$ | $a_{\mathrm{ww}}$ |
|---|---|---|---|---|---|---|---|---|---|---|---|
| 648 000 | 3 | 3 | 0.05 | 50 | 0.8 | 25 | 60 | 20 | 25 | 60 | 25 |

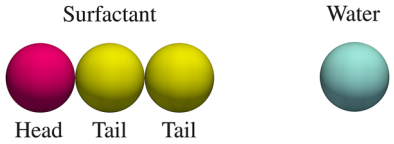


**FIG. 1.** Schematic of the coarse-grained model of a surfactant and water. The head of the former is a hydrophilic particle, and the tails are hydrophobic particles.

## C. Simulation details

To integrate the equations of motion, we use the modified velocity Verlet method,[35]

$$\begin{aligned} \boldsymbol{r}_i(t+\Delta t) &= \boldsymbol{r}_i(t) + \Delta t \boldsymbol{v}_i(t) + \frac{1}{2}(\Delta t)^2 \boldsymbol{F}_i(t), \\ \widetilde{\boldsymbol{v}}_i(t+\Delta t) &= \boldsymbol{v}_i(t) + \lambda \Delta t \boldsymbol{F}_i(t), \\ \boldsymbol{F}_i(t+\Delta t) &= \boldsymbol{F}_i(\boldsymbol{r}(t+\Delta t), \widetilde{\boldsymbol{v}}_i(t+\Delta t)), \\ \boldsymbol{v}_i(t+\Delta t) &= \boldsymbol{v}_i(t) + \frac{1}{2}\Delta t(\boldsymbol{F}_i(t) + \boldsymbol{F}_i(t+\Delta t)), \end{aligned} \tag{12}$$

where $\Delta t$ is the time step, $\boldsymbol{F}_i$ is the force exerted on the $i$th particle, $\lambda$ is the parameter introduced in this algorithm, and $\widetilde{\boldsymbol{v}}_i$ is the predicted velocity of the $i$th particle. The random force defined by Eq. (4) is expressed by

$$\boldsymbol{F}_{ij}^R = \sigma w_R(r_{ij}) \zeta_{ij} \Delta t^{-1/2} \boldsymbol{e}_{ij} \tag{13}$$

when we calculate Eq. (12). In Eq. (13), $\zeta_{ij}$ is a Gaussian random variable with zero mean and unit variance. According to Ref. 35, we choose $\lambda = 0.65$ and $\Delta t = 0.04$. We have confirmed that these parameters realize sufficiently accurate temperature control.

In the present study, we use the Lees–Edwards boundary condition[40] and the so-called SLLOD equations[41] to generate a uniform shear flow as shown in Fig. 2. The SLLOD equations read

$$\begin{aligned} \dot{\boldsymbol{r}}_i &= \boldsymbol{p}_i / m_i + \boldsymbol{r}_i \cdot \nabla \boldsymbol{u}, \\ \dot{\boldsymbol{p}}_i &= \boldsymbol{F}_i - \boldsymbol{p}_i \cdot \nabla \boldsymbol{u}, \end{aligned} \tag{14}$$

where $\boldsymbol{p}_i$ is the so-called peculiar momentum and $\boldsymbol{u}$ is the fluid stream velocity. In the case of a uniform shear flow, we can express $\nabla \boldsymbol{u}$ as

$$\nabla \boldsymbol{u} = \begin{pmatrix} 0 & 0 & 0 \\ \dot{\gamma} & 0 & 0 \\ 0 & 0 & 0 \end{pmatrix}, \tag{15}$$

with $\dot{\gamma}$ being the shear rate. We impose a random initial configuration and conduct equilibrium simulations for 20 000 time units,

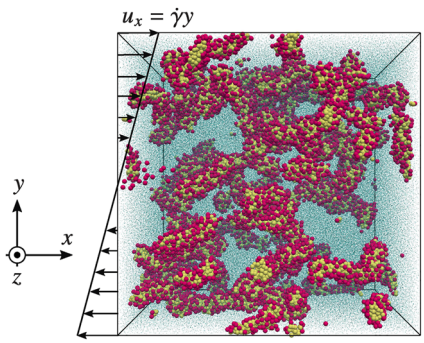


**FIG. 2.** Visualization of a system composed of surfactants and water. Hydrophilic and hydrophobic particles are indicated in red and yellow, respectively. For clarity, water particles are represented by blue dots.

achieving statistically steady values of the potential energy. After that, we conduct nonequilibrium simulations by imposing shear flow. We perform all the DPD simulations using our in-house code.

We define micelles adopting the method used in previous studies.[37,42] In this method, we judge that two surfactant molecules belong to a common cluster if a hydrophobic particle of one surfactant molecule is within $r_c(=1)$ of a hydrophobic particle of the other. If a cluster has an aggregation number $N_{ag}$ larger than a threshold value $n_{mic}(=10)$, then we regard the cluster as a micelle. Since we focus mainly on micelles with $N_{ag} \gtrsim 50$, our results are practically insensitive to the choice of $n_{mic}$. When we investigate the $N_{ag}$ dependence of micellar properties, we use conditional statistics based on $N_{ag}$. More concretely, to evaluate the micellar properties for a given $N_{ag}$, we use the data for micelles having aggregation numbers that lie in $[N_{ag} - \Delta N_{ag}, N_{ag} + \Delta N_{ag}]$, where we set $\Delta N_{ag} = 0.05 N_{ag}$.

## III. RESULTS AND DISCUSSION

### A. Timescales of micelles

One of the main goals of the present study is to elucidate the shear-rate dependence of flow-induced scission. For this purpose, we first identify the relevant timescales of micelles at equilibrium (i.e., in the absence of shear flow). As will be shown below, the rotational relaxation time $\tau_r$ and the average lifetime $\tau_b$ of micelles are the keys to understanding the dynamics of unentangled wormlike micelles under shear flow. More concretely, $\tau_r$ and $\tau_b$ determine their longest relaxation time $\tau$.

The target of the present study is the scission of rodlike and wormlike micelles. As shown in Appendix A, micelles are rodlike when $50 \lesssim N_{ag} \lesssim 200$ and wormlike when $N_{ag} \gtrsim 200$. To estimate $\tau_r$ of rodlike and wormlike micelles, we evaluate the rotational autocorrelation function,

$$C(t) = \left\langle \boldsymbol{e}^{(1)}(t_0 + t) \cdot \boldsymbol{e}^{(1)}(t_0) \right\rangle, \tag{16}$$

where $\boldsymbol{e}^{(1)}$ is the unit eigenvector of the gyration tensor $G_{ij}$ corresponding to the largest eigenvalue. Here, $G_{ij}$ is defined by

$$G_{ij} = \frac{1}{N_{sur}} \sum_{k=1}^{N_{sur}} \Delta r_{k,i} \Delta r_{k,j}, \tag{17}$$

where $\Delta r_{k,i}$ is the $i$th component of the relative position vector of the $k$th surfactant particle with respect to the center of mass of the micelle and $N_{sur}(=3N_{ag})$ is the number of surfactant particles in the micelle. Since $-\boldsymbol{e}^{(1)}$ is also a unit eigenvector of $G_{ij}$, we determine $\boldsymbol{e}^{(1)}(t)$ so that $\boldsymbol{e}^{(1)}(t - \delta t) \cdot \boldsymbol{e}^{(1)}(t) > 0$, where we set $\delta t = 100\Delta t$. Then we fit $C(t)$ with an exponential function,

$$C(t) = C_0 \exp(-t/\tau_r), \tag{18}$$

where $C_0$ is a constant, to determine $\tau_r$. Note that we use conditional statistics based on $N_{ag}$ to obtain $C(t)$ for a given $N_{ag}$. For each micelle, we evaluate $\boldsymbol{e}^{(1)}(t_0 + t) \cdot \boldsymbol{e}^{(1)}(t_0)$ until scission, which is defined below, occurs. We show in Fig. 3(a) that $C(t)$ can be expressed well by Eq. (18). Figure 3(b) shows $\tau_r$ as a function of $N_{ag}$. The slope of $\tau_r$ for $N_{ag} \gtrsim 200$ is smaller than that for $N_{ag} \lesssim 200$. Since as shown in Appendix A, rodlike micelles change into wormlike micelles above $N_{ag} \simeq 200$, micellar structures affect $N_{ag}$ dependence of $\tau_r$. As shown in Fig. 3(a), it is difficult to obtain $C(t)$ for large $N_{ag}$ with enough accuracy to estimate $\tau_r$. As discussed below, large micelles break into small micelles rapidly, thus making it difficult to acquire data for large $t$. Therefore, $C(t)$ for $N_{ag} = 400$ is shown within a limited range and fluctuates significantly for large $t$. As a result, the error bars of $\tau_r$ for large $N_{ag}$ are larger than those for small $N_{ag}$. However, in the case of the parameters used in the present study, the accuracy of $\tau_r$ for large $N_{ag}$ has little effect on the determination of the longest relaxation time introduced below.

Next, we investigate the characteristic timescale of micellar scission at equilibrium. Micelles repeatedly break and recombine due to the thermal effect. Here, we focus on the time required for micellar scission and evaluate the average lifetime $\tau_b$ of micelles at equilibrium. First, we explain how to detect the scission of micelles. We monitor $N_{ag}$ of each micelle at a certain time interval $\delta t(=100\Delta t)$, and when a micelle is decomposed into two or more groups, each of which contains more than $n_{mic}(=10)$ surfactant molecules, we consider that the micelle breaks. Then, we obtain the lifetime $t_b$ of each micelle. By conducting the analysis for different values of $n_{mic}$ in the range $5 \le n_{mic} \le 30$, we have confirmed that the choice of $n_{mic}$ has little effect on the following results. To describe the statistics of $t_b$, we investigate the survival function $S(t_b)$, which gives the probability that micelles survive beyond a certain time $t_b$. We estimate $S(t_b)$ using the Kaplan–Meier method.[43] Figure 4(a) shows $S(t_b)$ for several $N_{ag}$. We find that $S(t_b)$ obeys an exponential function, which means that micellar scission events occur with a constant probability per unit time. To obtain $\tau_b$, we fit $S(t_b)$ with $C_0 \exp(-t_b/\tau_b)$ except for short times where $S(t_b)$ does not show

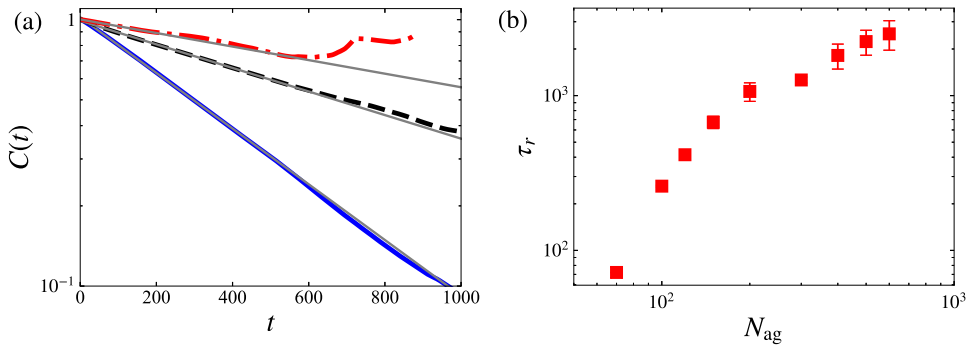


**FIG. 3.** (a) Rotational autocorrelation function $C(t)$ of micelles for $N_{ag} = 120$ (blue solid line), 200 (black dashed line), and 400 (red dotted-dashed line) at equilibrium with $k_BT = 1$. Gray lines are exponential fits to the data. (b) Rotational relaxation time $\tau_r$ of micelles as a function of $N_{ag}$ with $k_BT = 1$. The error bars in (b) denote the standard deviations for three independent simulations.

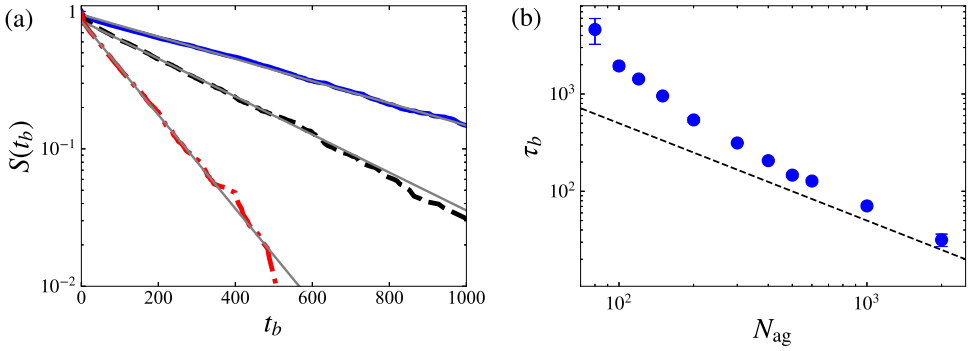


**FIG. 4.** (a) Survival function $S(t_b)$ of micelles for $N_{ag} = 200$ (blue solid line), 300 (black dashed line), and 600 (red dotted-dashed line) at equilibrium with $k_BT = 1$. Gray lines are exponential fits to the data. (b) Average lifetime $\tau_b$ of micelles as a function of the aggregation number $N_{ag}$ with $k_BT = 1$. The black dashed line indicates $\tau_b \propto N_{ag}^{-1}$. The error bars in (b) denote the standard deviations for three independent simulations.

an exponential decay. In Fig. 4(b), we show $\tau_b$ as a function of $N_{ag}$. Figure 4(b) shows $\tau_b \propto N_{ag}^{-1}$ for $N_{ag} \gtrsim 300$. This scaling is consistent with the model proposed by Cates,[23] which assumes that scission of chains occurs with a constant probability per unit time per unit length.

We have seen that $\tau_r$ is a monotonically increasing function of $N_{ag}$ [Fig. 3(b)], whereas $\tau_b$ is a monotonically decreasing function of $N_{ag}$ [Fig. 4(b)]. In Fig. 5(a), we show $\tau_r$ and $\tau_b$ as functions of $N_{ag}$ with $k_BT = 1$. These two timescales $\tau_r$ and $\tau_b$ cross each other at a certain aggregation number $N_\Lambda$ and we define $\tau_\Lambda$ as $\tau_r(N_\Lambda)$. Since $\tau_b(N_{ag}) < \tau_r(N_{ag})$ for $N_{ag} > N_\Lambda$ [Fig. 5(a)], the rotational relaxation of micelles with $N_{ag} \gtrsim N_\Lambda$ proceeds with the aid of scission. Here, note that $\tau_r$ corresponds to the rotational relaxation time of micelles without scission kinetics. In order to evaluate their longest relaxation time $\tau$ including the effect of scission kinetics, we extend the theory for the Rouse chain with the scission and recombination processes[24] to unentangled micelles. In contrast to the original theory, we do not assume that relaxation modes obey the Rouse theory. Instead, we use numerical results of $\tau_r$ and $\tau_b$ [Fig. 5(a)]. We then expect $\tau$ to follow

$$\tau(N_{ag}) = \begin{cases} \tau_r(N_{ag}) & (N_{ag} \lesssim N_\Lambda), \\ \tau_\Lambda & (N_{ag} \gtrsim N_\Lambda). \end{cases} \tag{19}$$

For $N_{ag} \lesssim N_\Lambda$, since $\tau_b$ is larger than $\tau_r$, the rotational relaxation of micelles is not affected by their scission, leading to $\tau(N_{ag}) = \tau_r(N_{ag})$. In contrast, for $N_{ag} \gtrsim N_\Lambda$, micelles can break into small micelles in a shorter time than $\tau_r(N_{ag})$. As a result, their rotational relaxation proceeds through that of these small micelles with a shorter relaxation time than $\tau_r(N_{ag})$. Similarly, the generated small micelles are likely to break into even smaller micelles before their rotational relaxation if $\tau_b < \tau_r$. Consequently, micelles such that $\tau_r \simeq \tau_b$ (i.e., $N_{ag} \simeq N_\Lambda$) determine the longest relaxation time. Therefore, micelles with $N_{ag} \gtrsim N_\Lambda$ relax with a characteristic time of the order of $\tau_\Lambda$ for which $\tau_r$ is comparable to $\tau_b$ [Fig. 5(a)]. This means that the slower relaxation timescales ($\tau_r > \tau_\Lambda$) disappear due to the rapid scission of large micelles with $N_{ag} \gtrsim N_\Lambda$. In other words, $N_\Lambda$ defines the largest segment that behaves in a similar way to polymer chains (i.e., chains without scission kinetics). This is why micelles with $N_{ag} \gtrsim N_\Lambda$ have a common longest relaxation time irrespective of $N_{ag}$. We show $\tau_\Lambda$ as a function of $1/k_BT$ in Fig. 5(b) and confirm the Arrhenius dependence. In addition, the inset in Fig. 5(b) shows that $N_\Lambda$ is also a monotonically increasing function of $1/k_BT$. To the best of our knowledge, this is the first evaluation of the longest relaxation time of unentangled surfactant micelles from the rotational relaxation time $\tau_r$ and the average lifetime $\tau_b$ using molecular simulations.

To confirm the validity of $\tau_\Lambda$ obtained by our extended method of Faivre and Gardissat,[24] we first examine the mean squared displacement (MSD) $\langle \Delta r^2 \rangle$ of surfactant molecules. Regarding polymer chains, the MSD of monomers is known to exhibit a subdiffusive regime when $t \lesssim \tau$ and a normal regime when $t \gtrsim \tau$ in DPD simulations,[44] where $\tau$ is the longest relaxation time of polymer chains. Huang *et al.*[21] reported that linear chains with a kinetic model for scission and recombination showed a similar crossover from subdiffusion to normal diffusion around $\tau_\Lambda$ obtained with the original method of Faivre and Gardissat.[24] We show the compensated MSD $\langle \Delta r^2 \rangle / t$ of surfactant molecules for various $k_BT$ as a function of $t/\tau_\Lambda$

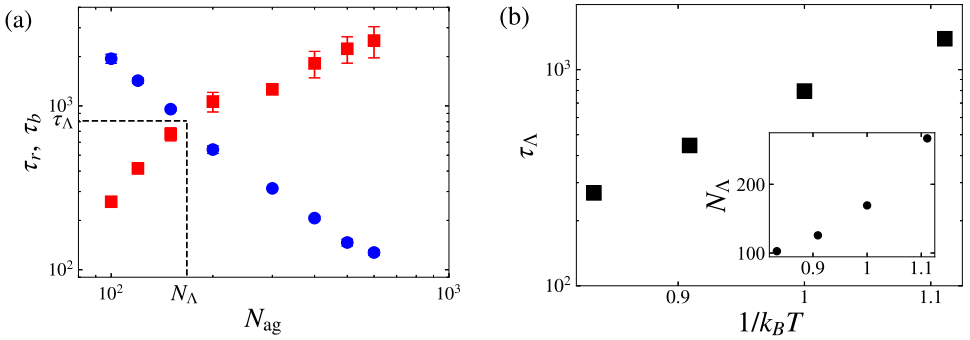


**FIG. 5.** (a) Rotational relaxation time $\tau_r$ (red square) and average lifetime $\tau_b$ (blue circle) as functions of the aggregation number $N_{ag}$ with $k_BT = 1$. Their intersection defines the longest relaxation time $\tau_\Lambda$ of micelles for $N_{ag} \gtrsim N_\Lambda$. The error bars denote the standard deviations for three independent simulations. (b) Longest relaxation time $\tau_\Lambda$ as a function of $1/k_BT$. The inset shows $N_\Lambda$ as a function of $1/k_BT$.

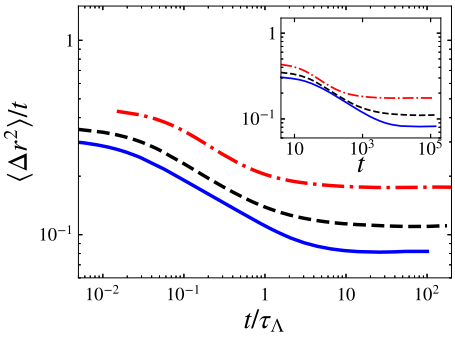


**FIG. 6.** Compensated MSD $\langle \Delta r^2 \rangle / t$ of surfactant molecules as a function of the normalized time $t/\tau_\Lambda$ with $k_BT = 0.9$ (blue solid line), $k_BT = 1$ (black dashed line), and $k_BT = 1.2$ (red dotted-dashed line). The inset shows $\langle \Delta r^2 \rangle / t$ as a function of $t$.

in Fig. 6. For $0.1 \lesssim t/\tau_\Lambda \lesssim 1$, $\langle \Delta r^2 \rangle / t$ has a negative slope, indicating the subdiffusion of surfactant molecules. In contrast, for $t/\tau_\Lambda \gtrsim 10$, $\langle \Delta r^2 \rangle / t$ is flat, indicating the normal diffusion. Thus, we confirm that $\langle \Delta r^2 \rangle$ shows a gradual crossover from subdiffusion to normal diffusion around $t/\tau_\Lambda = O(1)$, which is consistent with the property of the MSD in other systems mentioned above. For comparison, we show $\langle \Delta r^2 \rangle / t$ as a function of $t$ in the inset of Fig. 6. It is then more evident that $\tau_\Lambda$ serves as an appropriate timescale. However, $\langle \Delta r^2 \rangle$ includes the contribution from all the surfactant molecules, which belong to micelles of different sizes. We need to conduct a more detailed analysis of the MSD to directly prove the relevance of $\tau_\Lambda$, which is beyond the scope of the present study.

To summarize this section, we evaluated the longest relaxation time $\tau_\Lambda$ of unentangled surfactant micelles from the rotational relaxation time $\tau_r$ and the average lifetime $\tau_b$ of micelles at equilibrium by extending the concept proposed by Faivre and Gardissat.[24] We confirmed that the longest relaxation time serves as the relevant timescale at equilibrium by investigating the MSD. In Sec. III B, we focus on micelles with $N_{ag} \gtrsim N_\Lambda$ and verify the relevance of $\tau_\Lambda$ under shear flow by using conditional statistics based on $N_{ag}$.

## B. Flow-induced scission

In this section, we investigate the flow-induced scission of wormlike micelles under shear flow. We demonstrate that flow-induced scission occurs when the Weissenberg number $Wi_\Lambda = \tau_\Lambda \dot{\gamma}$ is larger than a threshold value.

To reveal the effect of flow-induced scission, we investigate the statistical properties of the micellar lifetime under shear flow. We show in Fig. 7(a) the survival function $S(t_b)$ of micelles for $N_{ag} = 300$ with $k_BT = 1$ for different $Wi_\Lambda$. For $Wi_\Lambda = 4.0$, $S(t_b)$ hardly differs from $S(t_b)$ at equilibrium ($Wi_\Lambda = 0$), whereas for $Wi_\Lambda = 8.0$ and 16, $S(t_b)$ declines with $Wi_\Lambda$. This indicates that, in addition to scission through thermal fluctuations, flow-induced scission occurs more significantly as $Wi_\Lambda$ increases. Figure 7(b) shows the $N_{ag}$ dependence of $\tau_b$ for the same $Wi_\Lambda$ as in Fig. 7(a). As shown in Fig. 7(a), for $Wi_\Lambda = 4.0$, the shear flow does not affect $\tau_b$ for any $N_{ag}$ considered here. In contrast, for $Wi_\Lambda = 8.0$ and 16, the shear flow reduces $\tau_b$ more significantly as $Wi_\Lambda$ increases. Note that $N_{ag}$ dependence of $\tau_b$ remains unchanged under shear flow for all $Wi_\Lambda$ considered here. In other words, the shear flow affects $\tau_b$ of micelles such that $N_{ag} \gtrsim N_\Lambda$ with a factor independent of $N_{ag}$. Figure 7(b) implies that the threshold value of $Wi_\Lambda$ for the decrease in $\tau_b$ is also independent of $N_{ag}$. Therefore, it is reasonable to conclude that micelles with $N_{ag} \gtrsim N_\Lambda$ have a common longest relaxation time, as explained in Eq. (19), and, consequently, their scission is promoted to the same degree by the shear flow.

Next, we demonstrate that $\tau_\Lambda$ defined as the value for which $\tau_r(N_{ag}) = \tau_b(N_{ag})$ [Fig. 5(a)] serves as the characteristic timescale in flow-induced scission. For this purpose, we consider several systems where $\tau_\Lambda$ takes different values by conducting DPD simulations with different $k_BT$ [Fig. 5(b)]. We show $\tau_b$ for $N_{ag} = 300, 400$, and 500 as a function of $Wi_\Lambda$ in Fig. 8. Here, $\tau_b$ is normalized by the value $\tau_b^0$ at equilibrium for a given $N_{ag}$. For comparison, we show $\tau_b/\tau_b^0$ as a function of $\dot{\gamma}$ in the inset of Fig. 8. The increase in

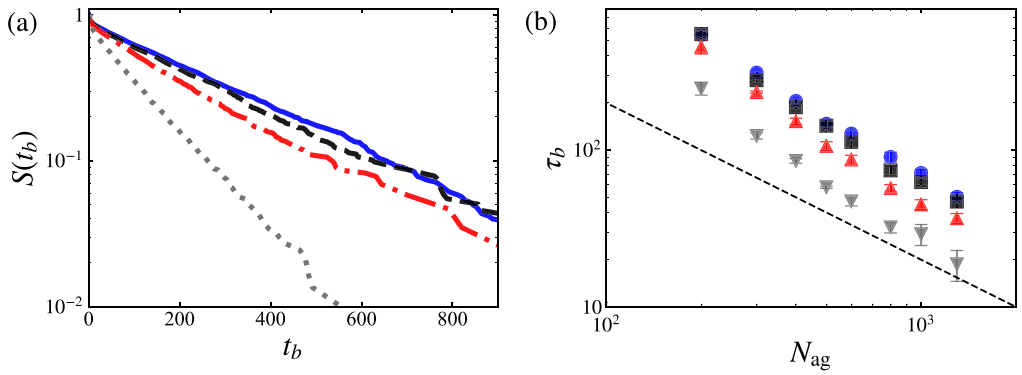


**FIG. 7.** (a) Survival function $S(t_b)$ of micelles with $N_{ag} = 300$ for $Wi_\Lambda = 0$ (blue solid line), 4.0 (black dashed line), 8.0 (red dotted-dashed line), and 16 (gray dotted line) with $k_BT = 1$. (b) Average lifetime $\tau_b$ of micelles as a function of the aggregation number $N_{ag}$ for $Wi_\Lambda = 0$ (blue circle), 4.0 (black square), 8.0 (red triangle), and 16 (gray inverted triangle) with $k_BT = 1$. The black dashed line in (b) indicates $\tau_b \propto N_{ag}^{-1}$. The error bars in (b) denote the standard deviations for three independent simulations.

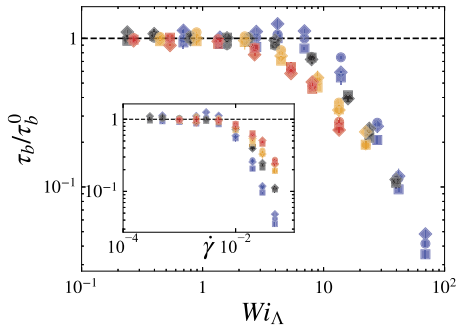


**FIG. 8.** Average lifetime $\tau_b$ normalized by the value $\tau_b^0$ at equilibrium as a function of the Weissenberg number $Wi_\Lambda$ for $N_{ag} = 300(\circ), 400(\square)$, and $500(\diamond)$ with $k_BT = 0.9$ (blue), 1 (black), 1.1 (orange), and 1.2 (red). The inset shows $\tau_b/\tau_b^0$ as a function of the shear rate $\dot{\gamma}$. The black dashed line indicates $\tau_b/\tau_b^0 = 1$. The error bars denote the standard deviations for three independent simulations.

$\tau_b/\tau_b^0$ with $k_BT$ for fixed $\dot{\gamma}$ indicates that scission of micelles is promoted more as the temperature is decreased for given $\dot{\gamma}$. In other words, the $\dot{\gamma}$ dependence of $\tau_b/\tau_b^0$ significantly differs depending on $k_BT$; micelles at a lower temperature are more likely to be broken by the shear flow. We emphasize that we can take into account this $k_BT$ dependence by using $\tau_\Lambda$. More concretely, all the data for different $k_BT$ as well as for different $N_{ag}$ follow a single function of $Wi_\Lambda$ (Fig. 8). The reason for this collapse is that micelles with $N_{ag} \gtrsim N_\Lambda$ are aligned and elongated by the shear flow with a timescale $\tau_\Lambda$, as we will discuss below (see Fig. 9). We have also confirmed that if $\phi \lesssim 0.1$, $\tau_b/\tau_b^0$ follows the same function shown in Fig. 8. Since $\phi$ does not significantly change the properties of micelles within the dilute regime, it is reasonable that $\tau_b/\tau_b^0$ is independent of $\phi(\lesssim 0.1)$. Interestingly, as shown in Fig. 8, $\tau_b \simeq \tau_b^0$ when $Wi_\Lambda$ is smaller than a threshold value $Wi_c(\simeq 4)$, indicating that flow-induced scission does not occur, whereas $\tau_b$ monotonically decreases with $Wi_\Lambda$ for $Wi_\Lambda > Wi_c$. However, it is difficult to discuss this

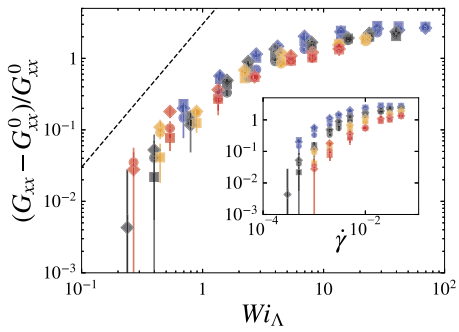


**FIG. 9.** Relative change $(G_{xx} - G_{xx}^0)/G_{xx}^0$ of diagonal component $G_{xx}$ of the gyration tensor normalized by the value $G_{xx}^0$ at equilibrium as a function of the Weissenberg number $Wi_\Lambda$ for $N_{ag} = 300(\circ), 400(\square)$, and $500(\diamond)$ with $k_BT = 0.9$ (blue), 1 (black), 1.1 (orange), and 1.2 (red). The black dashed line indicates $(G_{xx} - G_{xx}^0)/G_{xx}^0 \propto Wi_\Lambda^2$. The inset shows $(G_{xx} - G_{xx}^0)/G_{xx}^0$ as a function of the shear rate $\dot{\gamma}$. The error bars denote the standard deviations for three independent simulations.

threshold Weissenberg number $Wi_c$ in more detail due to the limited accuracy of $\tau_b$. We examine $Wi_c$ in another way, as described below (see Fig. 11). Since $\tau_r$ monotonically increases with $N_{ag}$ [Fig. 3(b)], it may be counterintuitive that the threshold shear rate for flow-induced scission is independent of $N_{ag}$ for fixed $k_BT$. As mentioned in Sec. III A, since the considered micelles satisfy $\tau_b(N_{ag}) < \tau_r(N_{ag})$ (i.e., $N_{ag} > N_\Lambda$), the slower relaxation timescales ($\tau_r > \tau_\Lambda$) disappear as a result of scission faster than the rotational relaxation, thus leading to a common threshold shear rate. In other words, the segment of size $N_\Lambda$ determines the effects of shear flow on micelles with $N_{ag} \gtrsim N_\Lambda$.

We investigate the gyration tensor defined by Eq. (17), which characterizes the micellar structure, to demonstrate that $\tau_\Lambda$ plays a vital role in the orientation and elongation of micelles under shear flow. Figure 9 shows the relative change $(G_{xx} - G_{xx}^0)/G_{xx}^0$ of the diagonal component $G_{xx}$ corresponding to the flow direction, where $G_{xx}^0$ is the value at equilibrium for fixed $N_{ag}$. All the data for different $k_BT$ and $N_{ag}$ approximately collapse on a single function of $Wi_\Lambda$, which indicates that $Wi_\Lambda$ determines the orientation and elongation of micelles under shear flow. This is consistent with the previous study,[25] which used linear chain models including scission and recombination kinetics. Therefore, we conclude that $Wi_\Lambda$ determines the effects of the shear flow on micelles, such as orientation and elongation, thus determining the degree of flow-induced scission, i.e., $\tau_b/\tau_b^0$, because the elongation of micelles causes their scission.[19,45] For comparison, we show $(G_{xx} - G_{xx}^0)/G_{xx}^0$ as a function of $\dot{\gamma}$ in the inset of Fig. 9. Without considering $\tau_\Lambda$, $(G_{xx} - G_{xx}^0)/G_{xx}^0$ depends on $\dot{\gamma}$ differently for each $k_BT$; its $\dot{\gamma}$ dependence varies greatly depending on $k_BT$. Therefore, $\tau_\Lambda$ is an important property for understanding the shear-rate dependence of the micellar dynamics under shear flow. In addition, $(G_{xx} - G_{xx}^0)/G_{xx}^0$ is independent of $N_{ag}$ for fixed $k_BT$ and $\dot{\gamma}$. This is consistent with our claim that micelles with $N_{ag} \gtrsim N_\Lambda$ have a common longest relaxation time for given $k_BT$. In Fig. 9, we find that $(G_{xx} - G_{xx}^0)/G_{xx}^0 \propto Wi_\Lambda^2$ holds for $Wi_\Lambda \lesssim 1$, which is a well-known characteristic of polymers.[46] This indicates that micelles behave similarly to polymers under shear flow for moderate $Wi_\Lambda$.

Here, note that $\tau_b/\tau_b^0$ and $(G_{xx} - G_{xx}^0)/G_{xx}^0$ do not completely follow a single curve, as shown in Figs. 8 and 9, indicating that there exist other relevant factors. For example, regarding semiflexible polymers, stiffness significantly affects their properties under shear flow.[47] In addition, although we do not consider the effect of branched micellar structures, these complex structures may also play a role in the micellar dynamics as demonstrated in a previous study.[48] Thus, topological characterization of micelles using the recently developed method[49] can provide valuable information about the detailed mechanism of flow-induced scission. This is an important near-future study.

We have seen that our analysis of the lifetime using conditional statistics clearly reveals how flow-induced scission affects individual micelles. Next, to examine how flow-induced scission affects the distribution of $N_{ag}$, we focus on the $Wi_\Lambda$ dependence of the probability density function $P(N_{ag})$ of $N_{ag}$. Figure 10 shows $P(N_{ag})$ for several values of $Wi_\Lambda$ with $k_BT = 1$. For $Wi_\Lambda < Wi_c(\simeq 4)$, $P(N_{ag})$ is independent of $Wi_\Lambda$. This indicates that flow-induced scission does not occur for $Wi_\Lambda < Wi_c$, which is consistent with the results shown in Fig. 8. For $Wi_\Lambda$ larger than $Wi_c$, in contrast, $P(N_{ag})$ for large $N_{ag}$ decreases and the distribution shifts to

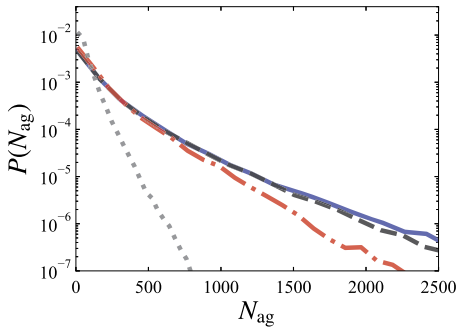


**FIG. 10.** Probability density function $P(N_{ag})$ of the aggregation number $N_{ag}$ for $Wi_\Lambda = 0$ (blue solid line), 4.0 (black dashed line), 8.0 (red dotted-dashed line), and 40 (gray dotted line) with $k_BT = 1$.

smaller $N_{ag}$ as $Wi_\Lambda$ increases. Therefore, it is clear that when $Wi_\Lambda$ exceeds $Wi_c$, flow-induced scission occurs, and then the population of large micelles declines. Note that for $Wi_\Lambda = 0$, $P(N_{ag})$ cannot be expressed by a single exponential function, whereas the model proposed by Cates[23] predicts the exponential distribution of micellar length. As shown in Fig. 4(b), micelles with $N_{ag} \lesssim 300$ do not satisfy the assumption that chains can break with a fixed probability per unit length per unit time. Therefore, it is reasonable that $P(N_{ag})$ does not obey a single exponential function, although we focus on $N_{ag}$ instead of micellar length. Dhakal and Sureshkumar[50] also reported that $P(N_{ag})$ did not obey an exponential function for charged micelles when the salt-to-surfactant concentration ratio was smaller than 1.

Before closing this article, we focus on the average number $\overline{N}_{mic}$ of micelles in the system and the mean aggregation number $\overline{N}_{ag}$, which reflect the onset of flow-induced scission, as discussed below. Figure 11(a) shows $\overline{N}_{mic}$ normalized by the value $\overline{N}^0_{mic}$ at equilibrium as a function of $Wi_\Lambda$. We find that $\overline{N}_{mic}/\overline{N}^0_{mic}$ is expressed by a single function of $Wi_\Lambda$ irrespective of $k_BT$. In addition, Fig. 11(a) provides clear evidence that flow-induced scission occurs for $Wi_\Lambda > Wi_c$ ($\simeq 4$). These observations are also valid for $\overline{N}_{ag}$ shown in Fig. 11(b). These results support the conclusion that $\tau_\Lambda$ is a relevant timescale of unentangled surfactant micelles. In the case of the parameters used in the present study, the average properties of the system, such as $\overline{N}_{mic}$ and $\overline{N}_{ag}$, are also determined by $Wi_\Lambda$. Since more than 65% of surfactants in the system belong to micelles with $N_{ag} \gtrsim N_\Lambda$ at equilibrium with $k_BT = 1$, it is quite reasonable that $\tau_\Lambda$ has a dominant influence on the average properties. Therefore, if we conduct experiments on the surfactant solutions where most surfactant molecules belong to micelles with $N_{ag} \gtrsim N_\Lambda$, the longest relaxation time $\tau_\Lambda$ will be a relevant timescale of the system. In other words, the experimentally obtained bulk properties such as viscosity are likely to be characterized by $\tau_\Lambda$. Indeed, as shown in Appendix B, $Wi_\Lambda$ determines the rheological properties of the considered solutions. Note that we take full advantage of molecular simulations to evaluate the longest relaxation time. We propose a method to obtain $\tau_\Lambda$ through the $N_{ag}$ dependences of $\tau_r$ and $\tau_b$, which are usually unavailable in experiments.

## IV. CONCLUSIONS

In the present study, we have investigated flow-induced scission of wormlike micelles in nonionic surfactant solutions under shear flow with DPD. Although flow-induced scission may be intuitively obvious, a quantitative understanding of this phenomenon has been unsatisfactory. This was mainly due to the difficulty of obtaining a large amount of micellar scission data for various aggregation numbers $N_{ag}$ and the lack of methods to estimate the relevant timescale of individual unentangled micelles. With the aid of the DPD method, which allows us to simulate large systems for long timescales, we can obtain a sufficient amount of data to discuss the statistical properties of micellar scission in detail.

In order to elucidate flow-induced scission in terms of micellar timescales, we have proposed a method to estimate the longest relaxation time $\tau_\Lambda$ of unentangled surfactant micelles from the rotational relaxation time $\tau_r$ (Fig. 3) and the average lifetime $\tau_b$ (Fig. 4) at equilibrium in the absence of shear flow. Using the concept proposed by Faivre and Gardissat,[24] which originally assumed the Rouse

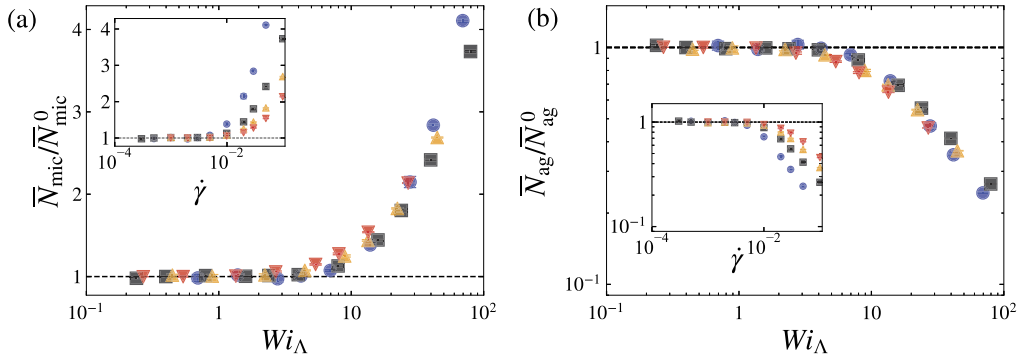


**FIG. 11.** (a) Average number $\overline{N}_{mic}$ of micelles in the system normalized by the value $\overline{N}^0_{mic}$ at equilibrium as a function of the Weissenberg number $Wi_\Lambda$. The black dashed line indicates $\overline{N}_{mic}/\overline{N}^0_{mic} = 1$. The inset shows $\overline{N}_{mic}/\overline{N}^0_{mic}$ as a function of the shear rate $\dot{\gamma}$. (b) Mean aggregation number $\overline{N}_{ag}$ normalized by the value $\overline{N}^0_{ag}$ at equilibrium as a function of $Wi_\Lambda$. The black dashed line indicates $\overline{N}_{ag}/\overline{N}^0_{ag} = 1$. The inset shows $\overline{N}_{ag}/\overline{N}^0_{ag}$ as a function of $\dot{\gamma}$. Different symbols correspond to different values of $k_BT$: blue circle, 0.9; black square, 1; orange triangle, 1.1; red inverted triangle, 1.2.

chain with scission and recombination processes, we have evaluated $\tau_\Lambda$ from the intersection of $\tau_r(N_{ag})$ and $\tau_b(N_{ag})$ [Fig. 5(a)]. This concept means that relaxation modes such that $\tau_r \gtrsim \tau_\Lambda$ disappear because the timescale of micellar scission is shorter than that of rotational relaxation for these modes. In fact, as shown in Fig. 6, the MSD of surfactant molecules has provided evidence that $\tau_\Lambda$ is a crucial timescale at equilibrium. More concretely, $\tau_\Lambda$ is comparable to the crossover time from subdiffusion to normal diffusion for different temperatures. These results are in agreement with the previous study using linear chains with a kinetic model for scission and recombination.[25] Thus, we have found that the concept proposed by Faivre and Gardissat[24] is also applicable to unentangled surfactant micelles when we develop the method to evaluate the longest relaxation time using data from molecular simulations.

One of the most important conclusions of the present study is that $\tau_\Lambda$ is a crucial timescale for flow-induced scission of wormlike surfactant micelles under shear flow. Our analysis relies on conditional statistics based on the aggregation number $N_{ag}$, which reveals the shear flow effect on individual micelles in detail. Indeed, the survival function $S(t_b)$ of micelles for fixed $N_{ag}$ has demonstrated that flow-induced scission occurs for high shear rates [Fig. 7(a)]. We have also found in Fig. 7(b) that for large $N_{ag}$, $\tau_b \propto N_{ag}^{-1}$ holds even under shear flow, similarly to the equilibrium state [Fig. 4(b)]. To demonstrate the role of $\tau_\Lambda$ in the shear-rate dependence of $\tau_b$, we have conducted DPD simulations for different temperatures. We have shown that the Weissenberg number $Wi_\Lambda$, which is defined as the product of the longest relaxation time $\tau_\Lambda$ and the shear rate $\dot{\gamma}$, determines $\tau_b$ under shear flow (Fig. 8). To the best of our knowledge, this is the first attempt to show that $\tau_b$ can be characterized by the nondimensionalized shear rate. Since $Wi_\Lambda$ also determines the diagonal component $G_{xx}$ of the gyration tensor $G_{ij}$ (Fig. 9), the $Wi_\Lambda$ dependence of $\tau_b$ is associated with the elongation of micelles. However, since the collapse is slightly unclear in Figs. 8 and 9, our numerical results suggest that, in addition to $Wi_\Lambda$, there exist other important factors, such as stiffness and branched micellar structures. We have examined the $Wi_\Lambda$ dependence of the micellar distribution (Fig. 10), the average number of micelles [Fig. 11(a)], and the average aggregation number [Fig. 11(b)]. We then conclude that flow-induced micellar scission occurs when $Wi_\Lambda$ is larger than a threshold Weissenberg number $Wi_c$. Although $Wi_c \simeq 4$ in the examined system, we speculate that $Wi_c$ depends on various factors, such as the conservative force coefficients $a_{ij}$ in the DPD method.

In the present study, we have revealed the shear-rate dependence of flow-induced scission focusing on nonionic surfactants. However, further studies are required. First, our results are restricted to the case of nonionic surfactant micelles. Regarding the scission of ionic surfactant micelles, we must consider the effect of counterions.[19] However, the proposed method to evaluate $\tau_\Lambda$ from $\tau_r$ and $\tau_b$ is applicable to molecular simulations of unentangled surfactant micelles regardless of the kind of surfactant. Thus, it is an interesting future study to investigate flow-induced scission of different kinds of surfactant micelles and reveal their differences, which will provide helpful insight into the practical applications of surfactant solutions. Second, we have not revealed the physical mechanism behind the statistical properties of flow-induced scission. To overcome this deficiency, it is necessary to reveal the dynamics of individual micelles, such as alignment and elongation.[19] Flow-induced scission is expected to have a great impact on micellar dynamics, thus leading to complicated behavior different from that of polymer chains (i.e., chains without scission kinetics). In addition, it is essential to understand flow-induced scission in terms of mechanics such as stress and energy.[18,19] Third, we should take into account the structural diversity in micelles. Here, we focused on conditional statistics based on aggregation numbers. However, as shown in Appendix A, micelles can form different structures even for a given aggregation number. It is, therefore, important to conduct a more detailed conditional analysis considering micellar structures.

## ACKNOWLEDGMENTS

The authors are grateful to Professor T. Inoue, Professor T. Kawakatsu, and Professor N. Matubayasi for valuable remarks on the first version of the manuscript. The present study was supported, in part, by the JSPS Grants-in-Aid for Scientific Research (Grant Nos. 20H02068 and 21J21061). The DPD simulations were mainly conducted under the auspices of the NIFS Collaboration Research Programs (Grant No. NIFS20KNSS145). A part of the simulations was conducted using the JAXA Supercomputer System Generation 3 (JSS3).

## AUTHOR DECLARATIONS

### Conflict of Interest

The authors have no conflicts to disclose.

### Author Contributions

**Yusuke Koide**: Conceptualization (equal); Data curation (lead); Formal analysis (lead); Investigation (lead); Methodology (equal); Validation (lead); Visualization (lead); Writing – original draft (lead); Writing – review & editing (equal). **Susumu Goto**: Conceptualization (equal); Funding acquisition (lead); Project administration (lead); Resources (lead); Supervision (lead); Writing – original draft (supporting); Writing – review & editing (equal).

## DATA AVAILABILITY

The data that support the findings of this study are available from the corresponding author upon reasonable request.

## APPENDIX A: STRUCTURAL PROPERTIES OF MICELLES AT EQUILIBRIUM

We adopt conditional statistics based on the aggregation number $N_{ag}$. In this appendix, we show the relationship between the micellar structure and $N_{ag}$.

First, we show snapshots of micelles for various $N_{ag}$ in Fig. 12, which qualitatively demonstrate how micelles grow with $N_{ag}$. Surfactants form spherical, rodlike, wormlike, and branched wormlike micelles as $N_{ag}$ increases. Note, however, that micelles can form various structures even for a given $N_{ag}$. In particular, for $N_{ag} \gtrsim 200$, both linear and branched micelles exist.

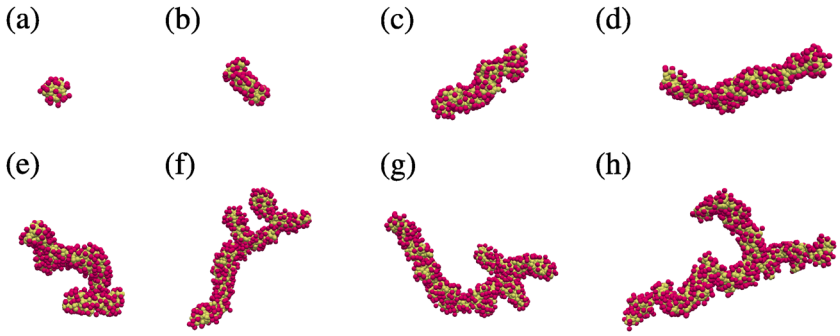


**FIG. 12.** Snapshots of micelles for (a) $N_{ag} = 40$, (b) 70, (c) 200, (d) 300, (e) 400, (f) 500, (g) 600, and (h) 700.

Next, to quantitatively investigate the structures of micelles, we focus on the gyration radius $R_g$ and relative shape anisotropy[51] $K^2$. These quantities are expressed as

$$R_g^2 = G_{xx} + G_{yy} + G_{zz} \tag{A1}$$

and

$$K^2 = 1 - 3\frac{G_{xx}G_{yy} + G_{yy}G_{zz} + G_{zz}G_{xx} - G_{xy}^2 - G_{yz}^2 - G_{zx}^2}{(G_{xx} + G_{yy} + G_{zz})^2} \tag{A2}$$

in terms of the gyration tensor $G_{ij}$ defined by Eq. (17). The relative shape anisotropy $K^2$ can take values between 0 and 1. A spherical structure is characterized by $K^2 \simeq 0$, and a rodlike structure is characterized by $K^2 \simeq 1$. Figure 13 shows $R_g$ and $K^2$ as functions of $N_{ag}$. Figure 13(a) shows that $R_g \propto N_{ag}^{1/3}$ for $N_{ag} \lesssim 50$. This behavior changes around $N_{ag} = 50$. Since $R_g \propto N_{ag}^{1/3}$ holds for spherical micelles,[31] the structural transition of micelles occurs around $N_{ag} = 50$. In addition, Fig. 13(b) demonstrates that $K^2 \simeq 0$ for $N_{ag} \lesssim 50$, and $K^2$ becomes much larger for $N_{ag} \gtrsim 50$. Therefore, micelles are spherical for $N_{ag} \lesssim 50$, whereas micelles are rodlike for $N_{ag} \gtrsim 50$. Note also a gradual decrease of $K^2$ for $N_{ag} \gtrsim 200$ [Fig. 13(b)]. This is because micelles for $N_{ag} \gtrsim 200$ are wormlike and flexible. These quantitative results are consistent with the visualizations of micellar structures shown in Fig. 12. Thus, $R_g$ and $K^2$ enable us to estimate the structure of micelles (i.e., spherical, rodlike, or wormlike). According to these criteria for micellar structures in terms of $N_{ag}$, we mainly deal with rodlike and wormlike micelles in the present study. We need to conduct a more detailed analysis to characterize branched structures. This is an important near-future study.

## APPENDIX B: RHEOLOGICAL PROPERTIES OF SURFACTANT SOLUTIONS

In this appendix, we show the rheological properties of the considered surfactant solutions. The stress tensor $\boldsymbol{\sigma}$ can be calculated using the Irving–Kirkwood equation,[52]

$$\boldsymbol{\sigma} = -\frac{1}{V}\left\langle \sum_{i=1}^{N} m\boldsymbol{v}_i\boldsymbol{v}_i + \sum_{i=1}^{N}\sum_{j>i}^{N} \boldsymbol{r}_{ij}\boldsymbol{F}_{ij} \right\rangle, \tag{B1}$$

where V is the volume of the system. Then, the viscosity $\eta$ and the first normal stress coefficient $\Psi_1$ are evaluated by

$$\eta = \frac{\sigma_{yx}}{\dot{\gamma}} \quad \text{and} \quad \Psi_1 = \frac{\sigma_{xx} - \sigma_{yy}}{\dot{\gamma}^2}, \tag{B2}$$

respectively. Figure 14 shows the $Wi_\Lambda$ dependences of $\eta$ and $\Psi_1$ for several $k_BT$. Here, $\eta$ is shown in the form of $(\eta - \eta_s)/(\eta_0 - \eta_s)$, where $\eta_s$ is the viscosity of water at a given $k_BT$ and $\eta_0$ is the viscosity of the solution at the lowest shear rate. The value of $\Psi_1$ is normalized by $\Psi_{1,0}$ at the lowest shear rate. Both $\eta$ and $\Psi_1$ decrease with $Wi_\Lambda$ when $Wi_\Lambda \gtrsim 1$. One might think that flow-induced scission causes this shear thinning. However, since the alignment of micelles in the flow direction also contributes to the shear thinning, a more detailed analysis is required to identify the effect of flow-induced scission on rheological properties. As shown in Fig. 14(b), the first normal stress

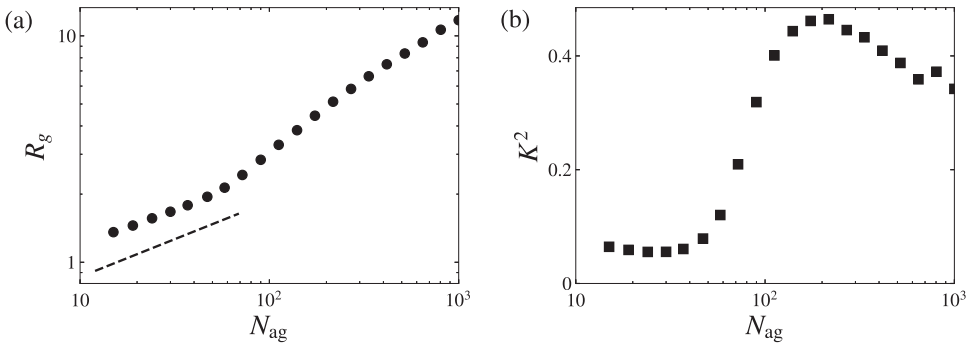


**FIG. 13.** (a) Gyration radius $R_g$ and (b) relative shape anisotropy $K^2$ as functions of the aggregation number $N_{ag}$ with $k_BT = 1$. The dashed line in (a) indicates $R_g \propto N_{ag}^{1/3}$.

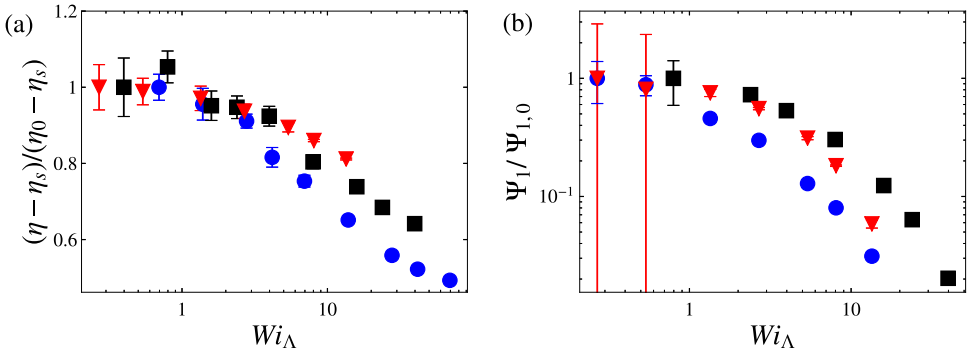


**FIG. 14.** (a) Increase in viscosity $\eta - \eta_s$ of the solutions from the solvent viscosity $\eta_s$ normalized by the value $\eta_0 - \eta_s$ at the lowest shear rate and (b) first normal stress coefficient $\Psi_1$ normalized by the value $\Psi_{1,0}$ at the lowest shear rate as functions of the Weissenberg number $Wi_\Lambda$. Different symbols correspond to different values of $k_BT$: blue circle, 0.9; black square, 1; red inverted triangle, 1.2. The error bars denote the standard deviations for three independent simulations.

difference is positive, indicating that the surfactant solutions have viscoelasticity.

## REFERENCES


[1]T. Shikata, H. Hirata, and T. Kotaka, "Micelle formation of detergent molecules in aqueous media: Viscoelastic properties of aqueous cetyltrimethylammonium bromide solutions," Langmuir **3**, 1081 (1987).

[2]Z. Chu, C. A. Dreiss, and Y. Feng, "Smart wormlike micelles," Chem. Soc. Rev. **42**, 7174 (2013).

[3]M. D. Warholic, G. M. Schmidt, and T. J. Hanratty, "The influence of a drag-reducing surfactant on a turbulent velocity field," J. Fluid Mech. **388**, 1 (1999).

[4]M. J. Lawrence, "Surfactant systems: Their use in drug delivery," Chem. Soc. Rev. **23**, 417 (1994).

[5]R. K. Prud'homme and G. G. Warr, "Elongational flow of solutions of rodlike micelles," Langmuir **10**, 3419 (1994).

[6]C.-M. Chen and G. G. Warr, "Light scattering from wormlike micelles in an elongational field," Langmuir **13**, 1374 (1997).

[7]J. P. Rothstein, "Transient extensional rheology of wormlike micelle solutions," J. Rheol. **47**, 1227 (2003).

[8]S. Chen and J. P. Rothstein, "Flow of a wormlike micelle solution past a falling sphere," J. Non-Newtonian Fluid Mech. **116**, 205 (2004).

[9]A. Kalb, L. A. Villasmil U., and M. Cromer, "Role of chain scission in cross-slot flow of wormlike micellar solutions," Phys. Rev. Fluids **2**, 071301 (2017).

[10]M. B. Khan and C. Sasmal, "Effect of chain scission on flow characteristics of wormlike micellar solutions past a confined microfluidic cylinder: A numerical analysis," Soft Matter **16**, 5261 (2020).

[11]P. A. Vasquez, G. H. McKinley, and L. P. Cook, "A network scission model for wormlike micellar solutions. I. Model formulation and viscometric flow predictions," J. Non-Newtonian Fluid Mech. **144**, 122 (2007).

[12]S. Dutta and M. D. Graham, "Mechanistic constitutive model for wormlike micelle solutions with flow-induced structure formation," J. Non-Newtonian Fluid Mech. **251**, 97 (2018).

[13]R. J. Hommel and M. D. Graham, "Constitutive modeling of dilute wormlike micelle solutions: Shear-induced structure and transient dynamics," J. Non-Newtonian Fluid Mech. **295**, 104606 (2021).

[14]S. J. Candau, F. Merikhi, G. Waton, and P. Lemaréchal, "Temperature-jump study of elongated micelles of cetyltrimethylammonium bromide," J. Phys. France **51**, 977 (1990).

[15]F. Kern, P. Lemarechal, S. J. Candau, and M. E. Cates, "Rheological properties of semidilute and concentrated aqueous solutions of cetyltrimethylammonium bromide in the presence of potassium bromide," Langmuir **8**, 437 (1992).

[16]I. Couillet, T. Hughes, G. Maitland, F. Candau, and S. J. Candau, "Growth and scission energy of wormlike micelles formed by a cationic surfactant with long unsaturated tails," Langmuir **20**, 9541 (2004).

[17]F. Liu, D. Liu, W. Zhou, F. Chen, and J. Wei, "Coarse-grained molecular dynamics simulations of the breakage and recombination behaviors of surfactant micelles," Ind. Eng. Chem. Res. **57**, 9018 (2018).

[18]T. Mandal and R. G. Larson, "Stretch and breakage of wormlike micelles under uniaxial strain: A simulation study and comparison with experimental results," Langmuir **34**, 12600 (2018).

[19]A. Sambasivam, A. V. Sangwai, and R. Sureshkumar, "Dynamics and scission of rodlike cationic surfactant micelles in shear flow," Phys. Rev. Lett. **114**, 158302 (2015).

[20]M. Kröger and R. Makhloufi, "Wormlike micelles under shear flow: A microscopic model studied by nonequilibrium-molecular-dynamics computer simulations," Phys. Rev. E **53**, 2531 (1996).

[21]C.-C. Huang, H. Xu, and J.-P. Ryckaert, "Kinetics and dynamic properties of equilibrium polymers," J. Chem. Phys. **125**, 094901 (2006).

[22]J. T. Padding, E. S. Boek, and W. J. Briels, "Dynamics and rheology of wormlike micelles emerging from particulate computer simulations," J. Chem. Phys. **129**, 074903 (2008).

[23]M. E. Cates, "Reptation of living polymers: Dynamics of entangled polymers in the presence of reversible chain-scission reactions," Macromolecules **20**, 2289 (1987).

[24]G. Faivre and J. L. Gardissat, "Viscoelastic properties and molecular structure of amorphous selenium," Macromolecules **19**, 1988–1996 (1986).

[25]C.-C. Huang, J.-P. Ryckaert, and H. Xu, "Structure and dynamics of cylindrical micelles at equilibrium and under shear flow," Phys. Rev. E **79**, 041501 (2009).

[26]P. J. Hoogerbrugge and J. M. V. A. Koelman, "Simulating microscopic hydrodynamic phenomena with dissipative particle dynamics," Europhys. Lett. **19**, 155 (1992).

[27]P. Español and P. Warren, "Statistical mechanics of dissipative particle dynamics," Europhys. Lett. **30**, 191 (1995).

[28]S. Yamamoto and S. Hyodo, "Mesoscopic simulation of the crossing dynamics at an entanglement point of surfactant threadlike micelles," J. Chem. Phys. **122**, 204907 (2005).

[29]N. Arai, K. Yasuoka, and Y. Masubuchi, "Spontaneous self-assembly process for threadlike micelles," J. Chem. Phys. **126**, 244905 (2007).

[30]S. Meng, J. Zhang, Y. Wang, X. Li, C. Wu, T. Hou, L. Xiao, and G. Lu, "Simulating the rheology of surfactant solution using dissipative particle dynamics," Mol. Simul. **41**, 772 (2015).

[31]R. L. Anderson, D. J. Bray, A. Del Regno, M. A. Seaton, A. S. Ferrante, and P. B. Warren, "Micelle formation in alkyl sulfate surfactants using dissipative particle dynamics," J. Chem. Theory Comput. **14**, 2633 (2018).

[32]H. Wang, X. Tang, D. M. Eike, R. G. Larson, and P. H. Koenig, "Scission free energies for wormlike surfactant micelles: Development of a simulation protocol, application, and validation for personal care formulations," Langmuir **34**, 1564 (2018).

[33]C. R. Wand, M. Panoukidou, A. Del Regno, R. L. Anderson, and P. Carbone, "The relationship between wormlike micelle scission free energy and micellar composition: The case of sodium lauryl ether sulfate and cocamidopropyl betaine," Langmuir **36**, 12288 (2020).

[34]Y. Kobayashi, H. Gomyo, and N. Arai, "Molecular insight into the possible mechanism of drag reduction of surfactant aqueous solution in pipe flow," Int. J. Mol. Sci. **22**, 7573 (2021).
[35]R. D. Groot and P. B. Warren, "Dissipative particle dynamics: Bridging the gap between atomistic and mesoscopic simulation," J. Chem. Phys. **107**, 4423 (1997).
[36]J. Li, J. Wang, Q. Yao, Y. Zhang, Y. Yan, and J. Zhang, "The biphasic effect of ABA triblock copolymers on the self-assembly of surfactants: Insight from dissipative particle dynamics," Mol. Syst. Des. Eng. **4**, 921 (2019).
[37]M.-T. Lee, R. Mao, A. Vishnyakov, and A. V. Neimark, "Parametrization of chain molecules in dissipative particle dynamics," J. Phys. Chem. B **120**, 4980 (2016).
[38]R. L. Anderson, D. J. Bray, A. S. Ferrante, M. G. Noro, I. P. Stott, and P. B. Warren, "Dissipative particle dynamics: Systematic parametrization using water-octanol partition coefficients," J. Chem. Phys. **147**, 094503 (2017).
[39]E. Lavagnini, J. L. Cook, P. B. Warren, M. J. Williamson, and C. A. Hunter, "A surface site interaction point method for dissipative particle dynamics parametrization: Application to alkyl ethoxylate surfactant self-assembly," J. Phys. Chem. B **124**, 5047 (2020).
[40]A. W. Lees and S. F. Edwards, "The computer study of transport processes under extreme conditions," J. Phys. C: Solid State Phys. **5**, 1921 (1972).
[41]D. J. Evans and G. Morriss, *Statistical Mechanics of Nonequilibrium Liquids* (Cambridge University Press, 2008).
[42]A. Vishnyakov, M.-T. Lee, and A. V. Neimark, "Prediction of the critical micelle concentration of nonionic surfactants by dissipative particle dynamics simulations," J. Phys. Chem. Lett. **4**, 797 (2013).
[43]E. L. Kaplan and P. Meier, "Nonparametric estimation from incomplete observations," J. Am. Stat. Assoc. **53**, 457 (1958).
[44]W. Jiang, J. Huang, Y. Wang, and M. Laradji, "Hydrodynamic interaction in polymer solutions simulated with dissipative particle dynamics," J. Chem. Phys. **126**, 044901 (2007).
[45]J. Gao, S. Li, X. Zhang, and W. Wang, "Computer simulations of micelle fission," Phys. Chem. Chem. Phys. **12**, 3219 (2010).
[46]C.-C. Huang, R. G. Winkler, G. Sutmann, and G. Gompper, "Semidilute polymer solutions at equilibrium and under shear flow," Macromolecules **43**, 10107 (2010).
[47]R. G. Winkler, "Conformational and rheological properties of semiflexible polymers in shear flow," J. Chem. Phys. **133**, 164905 (2010).
[48]S. Dhakal and R. Sureshkumar, "Anomalous diffusion and stress relaxation in surfactant micelles," Phys. Rev. E **96**, 012605 (2017).
[49]B. O. Conchuir, K. Gardner, K. E. Jordan, D. J. Bray, R. L. Anderson, M. A. Johnston, W. C. Swope, A. Harrison, D. R. Sheehy, and T. J. Peters, "Efficient algorithm for the topological characterization of worm-like and branched micelle structures from simulations," J. Chem. Theory Comput. **16**, 4588 (2020).
[50]S. Dhakal and R. Sureshkumar, "Topology, length scales, and energetics of surfactant micelles," J. Chem. Phys. **143**, 024905 (2015).
[51]D. N. Theodorou and U. W. Suter, "Shape of unperturbed linear polymers: Polypropylene," Macromolecules **18**, 1206 (1985).
[52]J. H. Irving and J. G. Kirkwood, "The statistical mechanical theory of transport processes. IV. The equations of hydrodynamics," J. Chem. Phys. **18**, 817 (1950).